Chemical Science

RSC Publishing

EDGE ARTICLE

View Article Online
View Journal | View Issue

Cite this: *Chem. Sci.*, 2013, **4**, 2971

A two-step approach to the synthesis of N@C_{60} fullerene dimers for molecular qubits†

Simon R. Plant,‡*[a] Martyn Jevric,[a] John J. L. Morton,[ab] Arzhang Ardavan,[b] Andrei N. Khlobystov,[c] G. Andrew D. Briggs[a] and Kyriakos Porfyrakis[a]

Received 9th February 2013
Accepted 7th May 2013

DOI: 10.1039/c3sc50395j

www.rsc.org/chemicalscience

We report the two-step synthesis of a highly soluble fullerene dimer, both for short reaction times and at the microscale. We apply this reaction scheme to starting materials that contain $^{15}N@C_{60}$ and $^{14}N@C_{60}$, and we demonstrate how, if applied to highly pure N@C_{60} in the future, this scheme may be used to produce $(^{14}N@C_{60})_2$ or $(^{15}N@C_{60})_2$ dimers in one step, and crucially $^{14}N@C_{60}$–$^{15}N@C_{60}$ dimers in a second step. Such dimers represent isolated electron spin pairs that may be used to demonstrate entanglement between the spins. Additionally, CW EPR spectroscopy of the $^{15}N@C_{60}$–C_{60} dimer in the solid state reveals permanent zero-field splitting (D = 14.6 MHz and E = 0.56 MHz).

1 Introduction

The controlled coupling of spin centres is essential when constructing an architecture for molecular spin-based quantum information processing (QIP).[1] A major challenge is to induce the requisite coupling between two adjacent spins, whilst protecting them from neighbouring spins and any unwanted environmental interactions. For molecular systems, chemical engineering offers a high degree of control over the spacing of spin centres, and *inter*-molecular couplings may be reduced by dispersal in a diamagnetic matrix.[2,3] Endohedral fullerenes – where atoms, ions or clusters are encapsulated in a carbon cage – are attractive as elements in a QIP architecture owing to their native spin properties.[4,5] Of particular interest is N@C_{60},[6] as quantum information can be stored faithfully using its electron spin for 0.25 ms (ref. 7) – longer than for any other molecule. In principle, two magnetically distinct N@C_{60} molecules can be conjoined to provide isolated spin pairs. However, the chemistry is hindered by the low yield of N@C_{60} to C_{60} (typically 10^{-4} to 10^{-5}) in the starting material, a protracted purification process[8] and the spin loss of the derivatives.[9,10] Consequently, there are only a small number of examples of N@C_{60} derivatization: several monomers,[9–15] an endohedral fullerene–porphyrin dyad[16] and three types of endohedral fullerene–fullerene dimer.[17,18,19] Recently, we succeeded in synthesizing a covalently linked $^{14}N@C_{60}$–$^{14}N@C_{60}$ dimer using highly enriched N@C_{60}.[20] However, all of the above involve $^{14}N@C_{60}$ with ^{15}N present only in natural abundance.

Although no isolated $^{15}N@C_{60}$ derivatives have been reported until now, the routes to both $(^{15}N@C_{60})_2$ and $^{14}N@C_{60}$–$^{15}N@C_{60}$ dimers ($I = 1$ for the ^{14}N nucleus and $I = 1/2$ for the ^{15}N nucleus) are worthy of exploration as such dimer molecules offer the potential to encode two quantum bits (qubits) of information in the electron spins. Such molecules may therefore enable a demonstration of controlled coupling and quantum entanglement between the electron spins. In addition, recent work has demonstrated the use of $^{15}N@C_{60}$ as a quantum memory element through the transfer of qubit states between its electron spin and nuclear spin,[21] thereby re-igniting interest in isotopically enriched nitrogen as a dopant in fullerenes.

Here, we present a synthetic scheme that yields a highly soluble fullerene monoadduct and a dimer for short reaction times and at the microscale, in order to limit losses of N@C_{60} under reflux conditions. This reaction, if applied to pure N@C_{60}, has the potential to yield a $(^{14}N@C_{60})_2$ or $(^{15}N@C_{60})_2$ dimer in one step, and a $^{14}N@C_{60}$–$^{15}N@C_{60}$ dimer in an additional step. We demonstrate the feasibility of this approach by applying the reaction to starting materials that contain $^{15}N@C_{60}$ and $^{14}N@C_{60}$. EPR spectroscopy of the $^{15}N@C_{60}$–C_{60} dimer provides information about the symmetry of the spin environment, which is in agreement with the NMR data of the undoped dimer analogue. The synthetic scheme presented here opens the way for future work in this area.

[a]*Department of Materials, University of Oxford, Parks Road, Oxford, OX1 3PH, UK. E-mail: s.r.plant@bham.ac.uk*

[b]*CAESR, The Clarendon Laboratory, Department of Physics, University of Oxford, OX1 3PU, UK*

[c]*School of Chemistry, University of Nottingham, University Park, Nottingham, NG7 2RD, UK*

† Electronic supplementary information (ESI) available: Experimental methods and characterization data, including mass, UV-vis-NIR, NMR spectra. See DOI: 10.1039/c3sc50395j

‡ Present address: Nanoscale Physics Research Laboratory, School of Physics and Astronomy, University of Birmingham, Birmingham, B15 2TT, UK.

2 Results and discussion

2.1 Synthesis

The overall strategy used for synthesis of N@C_{60} derivatives is first to develop the synthetic method and perform all characterization with C_{60}. Quantities of the N@C_{60} derivatives are simply too small to permit characterization other than by EPR spectroscopy. When developing the synthetic method, the stability of N@C_{60} is a major consideration, as the molecule loses its spin properties if the endohedral nitrogen escapes the fullerene cage due to photo- and thermally activated processes.[9,10] Photo-activated processes may be arrested simply by shielding N@C_{60} and its derivatives from light; however, given that dimerization is a thermally activated process, some heating of the reagents is necessary. Short reaction times are therefore advantageous because their use may limit the spin loss that has been observed for other dimer reactions involving N@C_{60}.[18,19] The reaction scheme, which is based on the Prato method,[22] is shown in Fig. 1. Reaction times and stoichiometry have been optimized such that, for short reaction times (2 min), a mixture of the monomer and the dimer is produced, while at longer reaction times (15 min) the dimer is favoured. The products are readily separated using high performance liquid chromatography (HPLC). The sidegroups incorporating an alkyl chain significantly enhance solubility in toluene and other solvents, which limits the loss of the products through precipitation during processing by HPLC. By thin layer chromatography, the dimer fraction consists of a diastereomeric mixture with approximately equal intensities, and this is consistent with the corresponding HPLC chromatogram (shown in Fig. 2). The stereoisomers are shown in the ESI.†

The optical absorption spectra for the C_{60}–C_{60} diastereomers are almost identical, exhibiting peaks in the visible region at wavelengths of 433 and 706 nm. The peak at 433 nm is indicative of the cycloaddition across a 6,6 ring junction of the fullerene cage.[15] A useful comparison is with the spectrum of C_{60}, because it has a characteristic absorption band in the range 440–700 nm which is absent for the dimer diastereomers, indicating that functionalization of the fullerene cage has taken place. The onset of absorption for the diastereomers occurs at around 740 nm, which corresponds to a HOMO–LUMO gap of 1.7 eV.

The merit of the scheme shown in Fig. 1 is that the monomer and dimer produced in Step 1 are readily separated, and the monomer can then be used to form the dimer in Step 2. Hence, this method could be use to produce an asymmetric dimer of

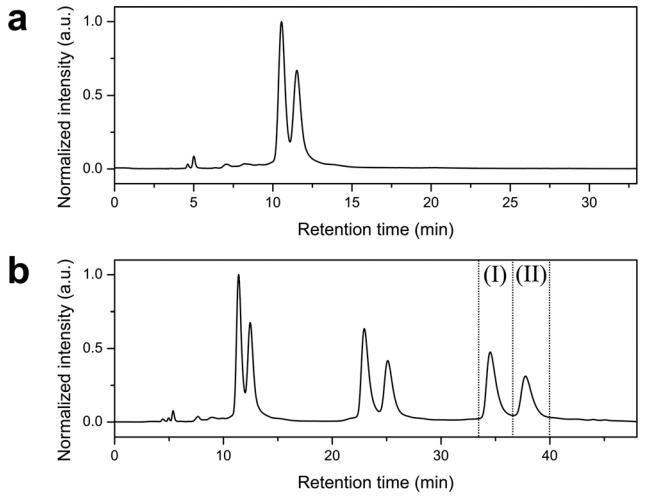

Fig. 2 Chromatograms showing the separation of the diastereomers of the C_{60}–C_{60} dimer (column: Buckyprep-M; eluent: toluene; flow rate: 18 ml min^{-1}). (a) Chromatogram revealing two peaks (only) from the dimer fraction, corresponding to the diastereomers. (b) Chromatogram showing separation of the two diastereomers using recycling HPLC (3 cycles). On the third cycle, the sample is divided into fractions (I) and (II) corresponding to the diastereomers (I) and (II), respectively. Minor impurities that appear before 10 minutes were removed during the first pass through the column.

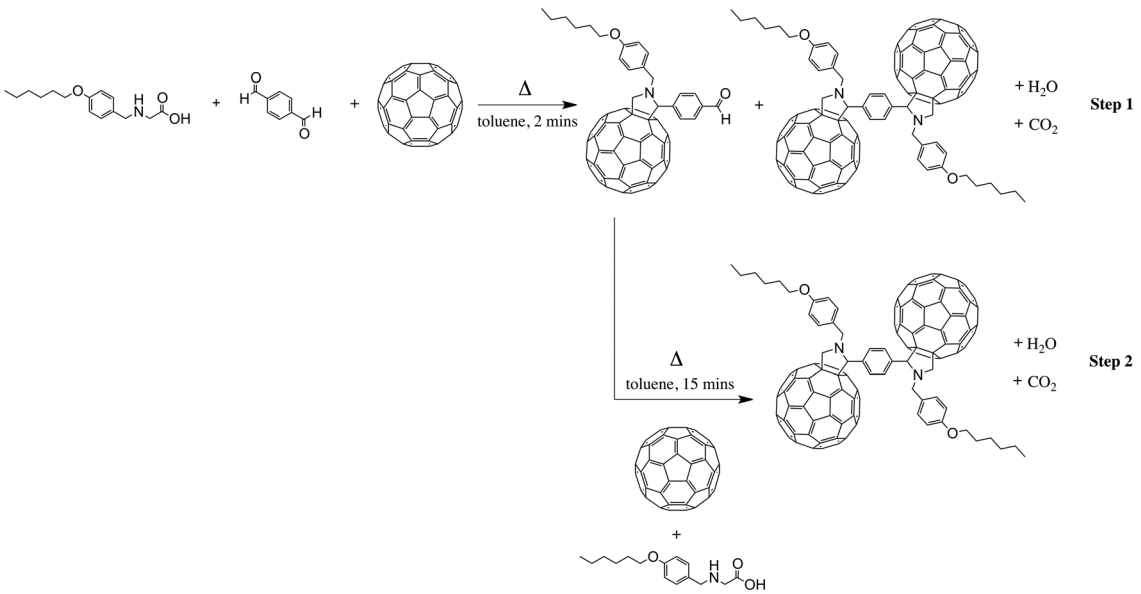

Fig. 1 Two-step procedure that affords a fullerene monomer and a fullerene dimer.

the type $^{14}N@C_{60}$–$^{15}N@C_{60}$ (illustrated by the proposed scheme in Fig. 3). We performed several microscale reactions on quantities of C_{60} as low as 6 μg, in order to test that the reaction could be applied to the sub-milligram quantities of high purity $N@C_{60}$ obtained through current production methods. Even at this scale, the peaks corresponding to the dimer diastereomers could be resolved in the HPLC chromatogram.

2.2 EPR spectroscopy

Fig. 3 shows how the scheme shown in Fig. 1 can be applied to highly enriched $^{14}N@C_{60}$ and $^{15}N@C_{60}$ in order to synthesize a symmetric $(^{14}N@C_{60})_2$ or $(^{15}N@C_{60})_2$ dimer in one step, and an asymmetric $^{14}N@C_{60}$–$^{15}N@C_{60}$ dimer in a second step. This is very challenging to realize in practice, as it may take many months or years to produce sufficient quantities of highly pure $^{14}N@C_{60}$ and $^{15}N@C_{60}$ using current techniques. In the mean time, we have applied this reaction scheme to $^{14}N@C_{60}$ and $^{15}N@C_{60}$ (produced using isotopically enriched nitrogen), both of purity 10^{-3}% ($N@C_{60}$ to C_{60}).

The chromatogram in Fig. 4 shows the separation of the products after the reaction shown in Step 1 of Fig. 1 was applied to $^{14}N@C_{60}/C_{60}$. The monomer isolated from this first step was then reacted with $^{15}N@C_{60}/C_{60}$ according to Step 2 of Fig. 1. The EPR spectra of fractions (I) and (II) – as marked on the chromatogram of Fig. 5(a) – are shown in Fig. 5(b), and correspond to the dimer diastereomers formed after this second step. Both spectra, acquired while the samples were in liquid solution at room temperature, exhibit the hyperfine lines of ^{14}N (triplet) and ^{15}N (doublet). The dimer fractions therefore contain mixtures of paramagnetic $^{14}N@C_{60}$–C_{60} and $^{15}N@C_{60}$–C_{60} dimers, as indicated in Fig. 5(c). The statistical probability of a $N@C_{60}$–$N@C_{60}$ dimer being formed in these reactions was $\leq 10^{-10}$; however, it is evident that, were high purity $N@C_{60}$ to be used in both steps, this reaction scheme could be used to synthesize a $^{14}N@C_{60}$–$^{15}N@C_{60}$ dimer. Furthermore, EPR measurements made on these dimer fractions indicated no reduction in the intensity of the hyperfine lines after a period of approximately one month following the reaction, suggesting no marked decay of these $N@C_{60}$ derivatives. The only protective measure taken was to store the samples in the dark: the samples were kept at room temperature in toluene and were not de-oxygenated. These findings indicate that the $N@C_{60}$ derivatives are stable dissolved in toluene when exposed to air and at ambient temperature.

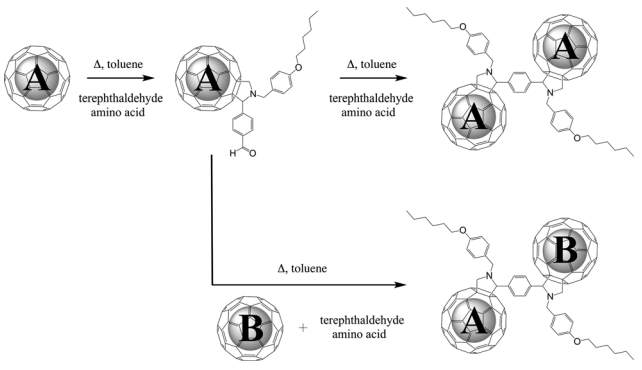

Fig. 3 Proposed reaction scheme for the synthesis of an asymmetric $^{14}N@C_{60}$–$^{15}N@C_{60}$ dimer in two steps based on the scheme shown in Fig. 1. In the first step (where A represents either ^{14}N or ^{15}N), the N-bearing monomer and symmetric dimer are formed. The second step yields an asymmetric $^{14}N@C_{60}$–$^{15}N@C_{60}$ dimer, whereby B represents either ^{14}N (if $^{15}N@C_{60}$ is used in the first step) or ^{15}N (if $^{14}N@C_{60}$ is used in the first step).

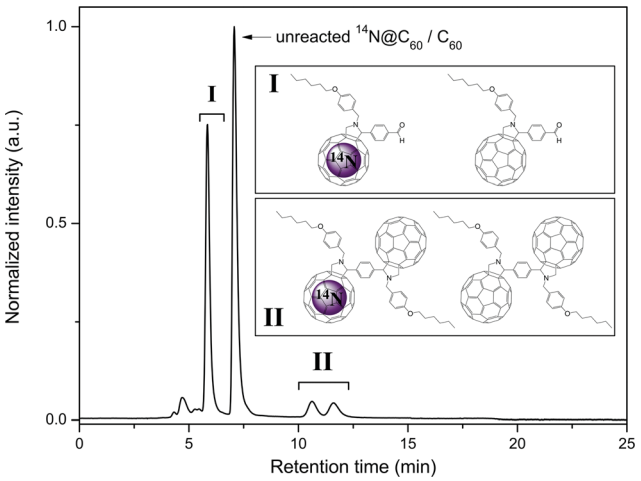

Fig. 4 Chromatogram showing the separation of monomer, dimer and unreacted $^{14}N@C_{60}/C_{60}$ following the application of the reaction shown in Step 1 of Fig. 1 to $^{14}N@C_{60}$ of purity 10^{-3}%.

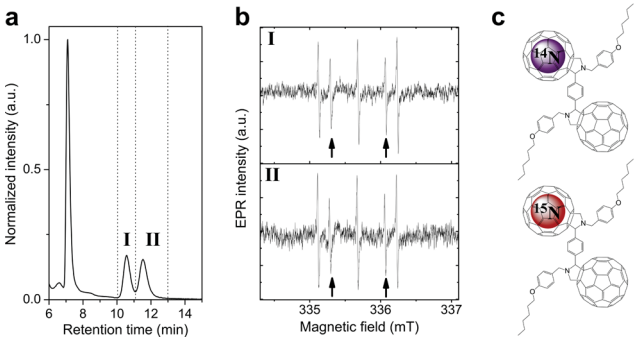

Fig. 5 (a) Chromatogram showing the separation of the dimer diastereomers (into fractions I and II) following the reaction of the $^{14}N@C_{60}/C_{60}$ monoadduct with $^{15}N@C_{60}/C_{60}$. (b) X-band CW EPR spectra corresponding to fractions I and II in solution at room temperature, both revealing the signals of endohedral ^{14}N (triplet) and ^{15}N (doublet, marked with arrows). (c) The paramagnetic $^{14}N@C_{60}$–C_{60} and $^{15}N@C_{60}$–C_{60} dimers present in fractions I and II.

We selected a diastereomeric mixture of the $^{15}N@C_{60}$–C_{60} dimer for further examination by continuous-wave (CW) EPR spectroscopy. The X-band CW EPR spectrum of the $^{15}N@C_{60}$–C_{60} dimer in the solid state (frozen toluene solution at 122 K) is shown in Fig. 6. The spectrum exhibits the hyperfine lines of ^{15}N corresponding to the $M_I = +1/2$ and $M_I = -1/2$ nuclear spin projections, as well as a distinct fine structure in the form of satellite peaks either side of these hyperfine lines. Peak-to-peak linewidths, Δl_{pp}, of the hyperfine lines are $\Delta l_{pp} = 1.07$ G. The hyperfine splitting, as measured directly between the $M_I = +1/2$ and $M_I = -1/2$ lines, is 22.1 MHz. By comparison, the isotropic hyperfine interaction of pristine $^{15}N@C_{60}$ is 22.021 MHz.[6] The sidepeaks flanking each hyperfine line are located 14.1 MHz from the line (also measured peak-to-peak). A further (weak)

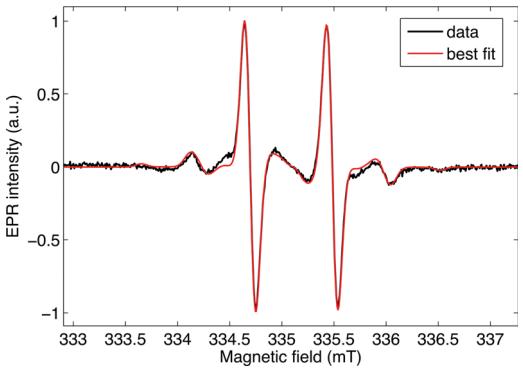

Fig. 6 X-band CW EPR spectrum of the $^{15}N@C_{60}$–C_{60} dimer in the solid state (frozen solution at 122 K). The best fit from the simulated model is shown in red.

sidepeak is also observed, located at 28 MHz upfield of the $M_I = -1/2$ line. The corresponding peak at 28 MHz downfield of the $M_I = +1/2$ line is obscured due to a locally rising baseline. The origin of this fine structure is attributable to *zero-field splitting* (ZFS), and these features are consistent with the fine structure observed in the powder spectra for $^{14}N@C_{60}$ derivatives.[12,14] For pristine $N@C_{60}$, the high spherical symmetry of the spin environment permits the endohedral nitrogen spin to be robust against many forms of decoherence. This is because high isotropy derives from the high spherical symmetry, leading to an isotropic *g*-factor, an isotropic hyperfine interaction and so forth.[23] Whenever the cage deviates from this high spherical symmetry, ZFS in the EPR spectrum is an inevitable consequence. For $N@C_{60}$, deviation from spherical symmetry occurs when the cage distorts. Distortions to the cage may arise temporarily through *inter*-molecular collisions, resulting in ZFS fluctuations, or they may be permanent, as is the case for functionalization with an adduct, which induces a permanent defect in the fullerene cage. This results in the deviation from spherical symmetry of the electron distribution surrounding the encapsulated nitrogen atom and, for frozen samples, an EPR spectrum characteristic of a small ZFS. ZFS is not observed in the EPR of samples in liquid solution because the molecules are tumbling rapidly, effectively restoring the spherical symmetry. Measuring the ZFS contribution can therefore confirm derivatization of the $N@C_{60}$ molecule and convey important information about the symmetry of the spin environment.

The ZFS is represented by the tensor, $\boldsymbol{D}$, which appears in the ZFS Hamiltonian. The $\boldsymbol{D}$-tensor is defined in terms of the parameters, D and E, the axial and rhombic components, respectively:[24,25]

$$\boldsymbol{D} = \begin{pmatrix} -\frac{1}{3}D + E & 0 & 0 \\ 0 & -\frac{1}{3}D - E & 0 \\ 0 & 0 & \frac{2}{3}D \end{pmatrix}$$

The parameter, D, represents the deviation from spherical symmetry – whilst the parameter, E, represents deviation from axial symmetry – of the electron density.[17] Consequently, for a system with high spherical symmetry of the electron density distribution, as for $N@C_{60}$, $D = 0$, $E = 0$. Axial symmetry leads to a non-zero D term: $D \neq 0$, $E = 0$. A simulated model was fitted to the solid-state EPR spectrum of the $^{15}N@C_{60}$–C_{60} dimer using *Easyspin*.[26] The best fit to the spectral data (see Fig. 6) is provided by the parameters associated with orthorhombic symmetry, with $D = 14.6$ MHz and $E = 0.56$ MHz, similar to previously reported $^{14}N@C_{60}$ derivatives.[15] This is consistent with the NMR data (see ESI†), which shows that the symmetry of the fullerene cages is lowered significantly. The $\boldsymbol{g}$-tensor can be essentially considered as isotropic, $g_{iso} = 2.0027$. There is, however, anisotropy in the hyperfine interaction, $\boldsymbol{A}$, with $A_{xx} = 22.6$, $A_{yy} = 21.7$ and $A_{zz} = 22.0$ MHz. This results from the anisotropy in the overlapping nuclear and electron wavefunctions, which is induced by the distortion of the fullerene cage.

3 Conclusions

In summary, we have developed a synthetic scheme to produce highly soluble, asymmetric fullerene dimers both for short reaction times and at the microscale. The high solubility is beneficial for processing, and limits losses of products through precipitation. By applying the reaction to starting materials containing $^{14}N@C_{60}$ and $^{15}N@C_{60}$, we have demonstrated that, if applied to highly pure $N@C_{60}$ in the future, this scheme may be used to yield $^{14}N@C_{60}$–$^{15}N@C_{60}$ dimers. Such molecules represent isolated spin pairs, which may be exploited for the purposes of demonstrating controlled coupling and quantum entanglement of the electron spins. EPR spectroscopy was performed on $^{15}N@C_{60}$–C_{60} dimers in the solid state, and the EPR spectrum exhibits zero-field splitting. The reaction scheme we have demonstrated offers the potential to synthesize spin-active dimers where each spin can be manipulated separately. This is an important step towards realising a molecular two-qubit system.

Acknowledgements

We acknowledge EPSRC funding (EP/F028806/01). S. R. P. acknowledges EPRSC for a Doctoral Training Award and for a PhD Plus Award. J. J. L. M., A. A. and A. N. K. are supported by the Royal Society.

References

1 A. Ardavan and S. J. Blundell, *J. Mater. Chem.*, 2009, **19**, 1754–1760.
2 Y. Ito, J. H. Warner, R. Brown, M. Zaka, R. Pfeiffer, T. Aono, N. Izumi, H. Okimoto, J. J. L. Morton, A. Ardavan, H. Shinohara, H. Kuzmany, H. Peterlik and G. A. D. Briggs, *Phys. Chem. Chem. Phys.*, 2010, **12**, 1618–1623.
3 M. Zaka, J. H. Warner, Y. Ito, J. J. L. Morton, M. H. Rümmeli, T. Pichler, A. Ardavan, H. Shinohara and G. A. D. Briggs, *Phys. Rev. B: Condens. Matter Mater. Phys.*, 2010, **81**, 075424.

4 W. Harneit, C. Meyer, A. Weidinger, D. Suter and J. Twamley, *Phys. Status Solidi B*, 2002, **233**, 453–461.
5 S. C. Benjamin, A. Ardavan, G. A. D. Briggs, D. A. Britz, D. Gunlycke, J. Jefferson, M. A. G. Jones, D. F. Leigh, B. W. Lovett, A. N. Khlobystov, S. A. Lyon, J. J. L. Morton, K. Porfyrakis, M. R. Sambrook and A. M. Tyryshkin, *J. Phys.: Condens. Matter*, 2006, **18**, S867–S883.
6 T. Almeida Murphy, Th. Pawlik, A. Weidinger, M. Höhne, R. Alcala and J.-M. Spaeth, *Phys. Rev. Lett.*, 1996, **77**, 1075–1078.
7 J. J. L. Morton, A. M. Tyryshkin, A. Ardavan, K. Porfyrakis, S. A. Lyon and G. A. D. Briggs, *J. Chem. Phys.*, 2006, **124**, 014508.
8 M. Kanai, K. Porfyrakis, G. A. D. Briggs and T. J. S. Dennis, *Chem. Commun.*, 2004, 210–211.
9 M. A. G. Jones, D. A. Britz, J. J. L. Morton, A. N. Khlobystov, K. Porfyrakis, A. Ardavan and G. A. D. Briggs, *Phys. Chem. Chem. Phys.*, 2006, **8**, 2083–2088.
10 G. Liu, A. N. Khlobystov, A. Ardavan, G. A. D. Briggs and K. Porfyrakis, *Chem. Phys. Lett.*, 2011, **508**, 187–190.
11 B. Pietzak, M. Waiblinger, T. Almeida Murphy, A. Weidinger, M. Höhne, E. Dietel and A. Hirsch, *Chem. Phys. Lett.*, 1997, **279**, 259–263.
12 E. Dietel, A. Hirsch, B. Pietzak, M. Waiblinger, K. Lips, A. Weidinger, A. Gruss and K.-P. Dinse, *J. Am. Chem. Soc.*, 1999, **121**, 2432–2437.
13 T. Wakahara, Y. Matsunaga, A. Katayama, Y. Maeda, M. Kako, T. Akasaka, M. Okamura, T. Kato, Y.-K. Choe, K. Kobayashi, S. Nagase, H. Huang and M. Ata, *Chem. Commun.*, 2003, 2940–2941.
14 L. Franco, S. Ceola, C. Corvaja, S. Bolzonella, W. Harneit and M. Maggini, *Chem. Phys. Lett.*, 2006, **422**, 100–105.
15 J. Zhang, J. J. L. Morton, M. R. Sambrook, K. Porfyrakis, A. Ardavan and G. A. D. Briggs, *Chem. Phys. Lett.*, 2006, **432**, 523–527.
16 G. Liu, A. N. Khlobystov, G. Charalambidis, A. G. Coutsolelos, G. A. D. Briggs and K. Porfyrakis, *J. Am. Chem. Soc.*, 2012, **134**, 1938–1941.
17 B. Goedde, M. Waiblinger, P. Jakes, N. Weiden, K.-P. Dinse and A. Weidinger, *Chem. Phys. Lett.*, 2001, **334**, 12–17.
18 J. Zhang, K. Porfyrakis, J. J. L. Morton, M. R. Sambrook, J. Harmer, L. Xiao, A. Ardavan and G. A. D. Briggs, *J. Phys. Chem. C*, 2008, **112**, 2802–2804.
19 F. Hörmann, A. Hirsch, K. Porfyrakis and G. A. D. Briggs, *Eur. J. Org. Chem.*, 2011, 117–121.
20 B. J. Farrington, M. Jevric, G. A. Rance, A. Ardavan, A. N. Khlobystov, G. A. D. Briggs and K. Porfyrakis, *Angew. Chem., Int. Ed.*, 2012, **51**, 3587–3590.
21 R. M. Brown, A. M. Tyryshkin, K. Porfyrakis, E. M. Gauger, B. W. Lovett, A. Ardavan, S. A. Lyon, G. A. D. Briggs and J. J. L. Morton, *Phys. Rev. Lett.*, 2011, **106**, 110504.
22 M. Maggini, G. Scorrano and M. Prato, *J. Am. Chem. Soc.*, 1993, **115**, 9798–9799.
23 J. J. L. Morton, Doctoral thesis, University of Oxford, 2005.
24 A. Schweiger and G. Jeschke, *Principles of Pulse Electron Paramagnetic Resonance*, Oxford University Press, Oxford, UK, New York, 2001.
25 A. Weidinger, M. Waiblinger, B. Pietzak and T. Almeida Murphy, *Appl. Phys. A: Mater. Sci. Process.*, 1998, **66**, 287–292.
26 S. Stoll and A. Schweiger, *J. Magn. Reson.*, 2006, **178**, 42–55.